The Land-Atmosphere Feedback Observatory: A New Observational Approach for Characterizing Land-Atmosphere Feedback

Florian Späth[1], Verena Rajtschan[2], Tobias K.D. Weber[2], Shehan Morandage[2], Diego Lange[1], Syed Saqlain Abbas[1], Andreas Behrendt[1], Joachim Ingwersen[2], Thilo Streck[2], Volker Wulfmeyer[1]

[1]University of Hohenheim, Institute of Physics and Meteorology, Stuttgart, Germany
[2]University of Hohenheim, Institute of Soil Science and Land Evaluation, Stuttgart, Germany

Correspondence to: Florian Späth (f.spaeth@uni-hohenheim.de)

Abstract. Important topics in Land-Atmosphere (L-A) feedback research are water and energy balances and heterogeneities of fluxes at the land-surface and in the ABL. To target these questions, the Land-Atmosphere Feedback Observatory (LAFO) has been installed in Southwest Germany. The instrumentation allows comprehensive and high-resolution measurements from the bedrock to the lower free troposphere. Grouped in three components: atmosphere, soil and land-surface and vegetation, the LAFO observation strategy aims for simultaneous measurements in all three compartments. For that the LAFO sensor synergy contains lidar systems to measure the atmospheric key variables humidity, temperature and wind. At the land-surface eddy covariance stations are operated to record the energy distribution of radiation, sensible, latent and ground heat fluxes. Together with a water and temperature sensor network the soil water content and temperature are monitored in the agricultural investigation area. In the vegetation crop height, leaf area index and phenological growth stage are registered.

The observations in LAFO are organized in operational measurements and intensive observation periods (IOPs). Operational measurements aim for long timeseries dataset to investigate statistics as we present as example the correlation between mixing layer height and surface fluxes. The potential of IOPs is demonstrated with a 24-hour case study with dynamic and thermodynamic profiles with lidar as well as a surface layer observation with the scanning differential absorption lidar to relate atmospheric humidity patterns to soil water structures.

Both IOPs and long-term observations will provide new insight into exchange processes and their statistics for improving the representation of L-A feedbacks in climate and numerical weather prediction models. Especially the lidar component will support the investigation of coupling to the atmosphere.

1 Introduction

Land-atmosphere (L-A) feedbacks are the result of interacting processes related to the exchange of momentum, energy, and mass in the L-A system. This system consists of the compartments soil, land cover such as vegetation, and the lower troposphere, encompassing the atmospheric boundary layer (ABL) and the surface layer (SL), including their modifications due to human activities.

A profound understanding and representation of L-A feedbacks contributes to an improvement of the skill of both weather (Holt et al. 2006) and medium-range to sub-seasonal forecasts (van den Hurk et al., 2012). L-A feedbacks have been identified as one of the key science topics for advancing regional climate simulations (Jacob et al., 2020). Dirmeyer et al. (2018) found clear underrepresentation of the feedback of surface fluxes on boundary layer properties (atmospheric coupling leg) and an overrepresentation of the connection between soil moisture and surface fluxes (terrestrial leg). L-A feedbacks influence the effects of historic, current, and future land use and land cover changes (LUCC) on regional hydrology, weather, and climate (Davin et al., 2020; Devanand et al., 2020; Stephens et al., 2021). It is of particular importance to understand these interactions over agricultural landscapes in order to maintain high crop yields and food security (Singh et al. 2018, McDermid et al. 2019). L-A feedbacks over agricultural landscapes are also critically important because they modify the impacts of climate change over land (Seneviratne et al., 2006, 2010; Dirmeyer et al., 2012). In the evolution and strength of heatwaves and droughts (Jaeger and Seneviratne, 2011; Zhou et al. 2019a; Miralles et al., 2014, 2019) L-A feedbacks play a very important role. These extremes are expected to be sensitive to and amplified by climate change (Vogel et al., 2017, 2018; IPCC 2021) and can only be simulated correctly if the feedbacks and reactions of the vegetation due to water and heat stress are well understood (Nolan et al., 2018; Anderegg et al., 2019; Zhou et al., 2019b). Advanced understanding of L-A feedback enables to consider bio-geoengineering efforts for mitigating the impacts of climate change (e.g., Davin et al., 2014; Branch and Wulfmeyer, 2019).

At any time and location, the quantities of the variables characterizing the L-A system such as the soil, canopy, and ABL temperatures and moistures as well as their fluxes and partitioning at the land surface are a result of these feedback processes (Santanello et al., 2018; Wulfmeyer et al., 2018; Helbig et al., 2021). With a typical depth ranging from several 100 m during night time to several km during the daytime, particularly the convective ABL (CBL) plays a very important role, as it rapidly responds (30-60 min) to changes of land surface properties by vertical mixing (Betts, 2004; Ek and Holtslag, 2004). For instance, van Heerwaarden et al. (2009) demonstrated that dry air entrainment in the CBL increases surface evaporation under all conditions. The strength of the L-A coupling depends on the incoming radiation, the land surface properties, and the large-scale synoptic forcing. Therefore, improved understanding of L-A feedbacks requires resolving its diurnal cycle and comprehending how it depends upon large-scale conditions and the evolving land cover over a vegetation period. These interactions become particularly complex when clouds and precipitation develop, feeding back to soil moisture, vegetation photosynthesis and the surface energy balance (e.g., Betts et al., 2007; Gentine et al., 2013; Vilà-Guerau de Arellano et al., 2014; Chen and Dirmeyer, 2017).

To improve the understanding of the feedback processes, observations of energy and water fluxes in the soil and at the land surface are necessary. L-A interactions at the surface are studied globally based on observations using eddy covariance (EC) stations. Many stations are organized in networks, e.g., FLUXNET (Baldocchi et al., 2001), AmeriFlux (Novick et al., 2018), ICOS (Franz et al., 2018), or TERENO (Zacharias et al., 2011) for which long-term dataset are available. Helbig et al. (2021) recently recommended to extent these observational stations with instruments for atmospheric measurements, which will certainly facilitate better understanding of the feedback of the land surface with the ABL and the lower free troposphere.

65   In addition to ground-based EC stations, remote sensing systems from aircraft or satellites can also observe the land surface. Measurements of atmospheric variables with high temporal and spatial resolutions, however, are even more challenging. Fields of wind, temperature, and moisture must be provided at the same time, as these variables are entangled in all standard SL schemes. Recently, a synergy of scanning lidar systems for wind, temperature and water-vapor became available fulfilling these measurement needs. For high-resolution line-of-sight wind measurements Doppler lidar (DL) systems use the

70   coherent detection technique. The required range-resolved temperature measurements are realized with temperature rotational Raman lidar (TRL) (Hammann et al., 2015; Behrendt et al., 2015, 2020) and the necessary measurements of the moisture field are provided either from a water-vapor Raman lidar (WVRL) (Turner et al., 2002; Wulfmeyer et al., 2010) or from a water-vapor differential absorption lidar (WVDIAL) (Wulfmeyer, 1999; Wagner et al., 2013; Wulfmeyer et al., 2016; Muppa et al., 2016; Späth et al., 2016). It was demonstrated that fluxes at the land surface and in the ABL can be measured.

75   Tests of model parameterizations against lidar observations was executed by Milovac et al. (2016) and Muppa et al. (2016). In 2017, the land-atmosphere feedback experiment (LAFE, Wulfmeyer et al., 2018) was, to the best of our knowledge, the first dedicated experiment to investigate L-A feedback with the deployment of a novel scanning lidar synergy. It took place at the ARM Southern Great Plains site in Oklahoma, USA, and complemented the existing suit of instruments with a combination of Doppler lidars, Raman lidars, and differential absorption lidars to measure the wind velocity, humidity, and

80   temperature from the land-surface through the ABL up to the lower troposphere (Späth et al., 2022; Lange et al., 2022). Operating scanning lidars were the key to obtain measurements in the surface layer region to overcome the near-range gap of vertical pointing lidars which deliver no data within the surface layer (Späth et al., 2022).

The campaign-based observations are time limited, thus, allow only few meteorological situations to be captured. For statistically significant results and robust conclusions, long-term observations are required. For that reason, the Land-

85   Atmosphere Feedback Observatory (LAFO) was set up as a research facility at the University of Hohenheim in Southwest Germany. The measurement data are comprehensive, highly resolved, and very precise, so that new parameterizations of land-atmosphere exchange processes between soil, vegetation and the lower troposphere can be developed, implemented, and tested (e.g. the applicability of the Monin-Obukhov similarity theory (MOST) for natural heterogeneous terrain). The design and operation of LAFO is connected to an international project of the World Climate Research Program (WCRP)

90   within the Global Land/Atmosphere System Study (GLASS) panel (see www.gewex.org/panels/global-landatmosphere-system-study-panel) named the Global Energy and Water Exchanges (GEWEX) LAFO (GLAFO, Wulfmeyer et al., 2020).

The overarching scientific goal of LAFO is to explore the L-A feedback with a novel synergy of energy balance/eddy covariance stations, soil and vegetation measurements, and scanning lidar systems. LAFO is a platform to bring together existing and unique instruments to seek for observations of the soil, the land surface, the vegetation and the lower

95   troposphere simultaneously.

To achieve the overarching goal, LAFO follows three scientific objectives:

1.   Determine the water and energy balances, and the land-atmosphere feedback as a function of the conditions of the soil, vegetation, and atmosphere in a study region with agricultural fields.

2.   Investigate the heterogeneity of the fluxes at the land surface and in the boundary layer.

100   3.   Develop new parameterizations of the fluxes at the land surface taking into account the vegetation dynamics and the turbulence in the ABL.

The LAFO measurement design follows the LAFE instrumentation and benefits from previous projects, e.g., the research unit "Agricultural Landscapes under Global Climate Change – Processes and Feedbacks on a Regional Scale" of the German

105   research foundation with long-term and on-going EC observations in Kraichgau and Swabian Jura area, southwestern Germany (Wizemann et al., 2015; Weber et al., 2022). This project contained also the Surface-Atmosphere-Boundary-Layer Exchange (SABLE) field campaign to test lidar observations in the surface layer (Späth et al., 2016). Both the LAFE and the new LAFO design with their instrument synergies have already made important contributions to this. Comparing observations to models, e.g. the applicability of MOST for natural heterogeneous land surfaces can be investigated or new

110   model parameterizations can be developed (Lee et al, 2019, 2020; Späth et al., 2022).
This paper presents LAFO: the observation strategy of the LAFO setup with the study area and its sensor synergy (section 2), the instrumentation (section 3) and, measurement examples (section 4). Finally, we summarize and give an outlook on future developments.

2 Observation Strategy

115

We aim for a synergistic sensor network, to simultaneously monitor a wide variety of system properties and state variables from bedrock to lower free troposphere to accomplish our LAFO objectives. The sensor synergy consists of the three components: 1) atmospheric measurements, 2) land-surface measurements, and 3) vegetation measurements. The interactions between the components are depicted in Figure 1 and the measured variables are listed in Table 1. The

120   observations illustrated in Figure 1 show the envisioned full suite of instrumentation for the full extent of observations to study L-A feedbacks as proposed by the GLASS panel. To observe the ABL and the interfacial layer the combination of scanning lidars play an important role to capture the relevant variables with required resolutions to resolve the processes. In the surface layer EC stations with 2 and 10 m measurement levels with several meteorological measurements can be complemented by temperature sensing along optical fibers (FODS) and low elevation scanning lidars. In the sub-surface and

125   soil regime measurements of soil moisture, temperature, matric potential and their profiles are important variables. Here several hydrological observations complement the information to characterize soil properties. The evapotranspiration of soil and vegetation can be sampled with the eddy-covariance method or lysimeters. To determine the contributions of soil and vegetation further measurements are helpful such as sap flow or other vegetation characterizing measurements. It is noted that some depicted measurements can be obtained continuously and perhaps automated while others are obtained better

130   during field experiments and intensive observation periods (IOPs).

In the following, we explain the target variables and introduce the sensor synergy and our experimental site. The available and operated instruments in LAFO are described in Sect. 3.

2.1 Targeted Variables

The key atmospheric variables absolute humidity q, temperature θ, and the turbulent fluctuations of the vertical wind w are captured with resolutions of 1-10 s in time and 30-60 m in space. The same holds for the by-products aerosol particle backscatter and extinction coefficient (β_{par}, α_{par}) and their optical thickness (τ_{par}), as well as the instantaneous boundary layer height $z_i(t)$. Furthermore, the horizontal wind profile $U(z)$ and potential properties like the atmospheric optical thickness τ_C can be retrieved. The combination of these variables delivers the following values: the dissipation of the turbulent kinetic energy (TKE) ε, profiles of the latent and sensible heat fluxes $L=<w'q'>$, $S=<w'\theta'>$ and the variances, $<q'^2>$, $<\theta'^2>$, and $<w'^2>$, mixed terms of higher orders like $<w'q'^2>$ and the molecular destruction rate of humidity and temperature ε_q and ε_θ (Wulfmeyer et al., 2016, 2022a) which are fundamental for budget analyses. Uncertainties of these variables are separated in atmospheric variance and instrumental noise with the autocovariance method described in Lenschow et al. (2000), Turner et al. (2014), and Wulfmeyer et al. (2016). The shear velocity $u*$ and the surface latent and sensible heat fluxes L_0 and S_0, the convective scales of vertical wind, humidity and temperature $w*$, $q*$, $\theta*$ are determined by combining the scanning lidars with MOST (Späth et al., 2022) or EC station measurements with MOST (Wulfmeyer et al., 2022b).

To study vegetation status and spatial pattern in standing crops we will record information about biomass, plant height z_p, plant density ρ_P, plant humidity content q_P, skin temperature T_S of bare soil, normalized difference vegetation index (NDVI), leaf area index (LAI) and nitrogen supply (red edge inflection point, REIP). The vegetation development status is registered according to the BBCH scale (Biologische Bundesanstalt für Land- und Forstwirtschaft, Bundessortenamt und Chemische Industrie; Meier, 2018). The temporal dynamics and spatial configuration of the vegetation state is characterized routinely by LAI measurements and management data are provided by the field index cards of the agricultural plots. For the sub-surface characterization of root growth dynamics, root density distribution, and root water uptake at various soil depths, additional field campaigns can be applied to complete the full picture.

The Water and Temperature Sensor Network (WaTSeN) monitors the spatial variability of soil water content $q(-z)$ and soil temperature $\theta(-z)$ in 40-cm depth. We cover an area of 0.84 km^2 with our sensory and record with a 15-minute interval. Additionally, the surface energy balance is investigated at two locations by measuring the surface sensible and latent heat fluxes S_0 and L_0, the ground heat flux G and the net radiation Q_n. Also, the evaporation of the footprint can be derived from these data to identify energy balance errors of the EC stations (Ingwersen et al, 2015; Imukova et al., 2016). Profiles of soil water content $q(-z)$, soil temperature $T(-z)$ and matric potential $h(-z)$ are measured at the EC stations. The variability of the soil properties can be studied with soil samples, geophysical (e.g. EM38) and agricultural measurements (e.g. traction measurements during tillage, Schutte, 2005).

With these data, the scientific objectives of LAFO can be achieved in the following way:

I. Determination of the water and energy balances and the LA feedback as a function of soil, vegetation, and atmospheric conditions in an agricultural study area. By combining the measurements of the LAFO components 1 and 2, all terms of the water vapor budget can be measured. Thus, the evolution of the boundary layer can be related to the state of the soil and the vegetation (LAFO component 3). This coupling of variables under different atmospheric conditions is sought (e.g., Dirmeyer, 2014) to understand and predict changes in the components of the water budget, including clouds and precipitation due to internal and external factors (e.g., climate change) in the region. These data will also be used to help determine the accuracy of models in simulating the coupling.

II. Investigation of the heterogeneity of fluxes at the land surface and in the boundary layer: The usual neglect of the heterogeneity of the fluxes leads to errors in weather prediction and climate models. When these heterogeneities are resolved, new scaling approaches can be developed and their impact on the coarse-scale used in models can be investigated. Furthermore, measuring the states of the land surface and boundary layer at the aimed high resolution will allow us to address the closure problem of EC measurements (Mauder et al., 2020; Ingwersen et al. 2015). A quantitative solution to the energy balance closure problem would enhance the confidence in the data from the international eddy covariance networks (e.g., FLUXNET) when being used for model validation.

III. Development of new parameterizations of the fluxes at the land surface under consideration of vegetation dynamics as well as turbulence in the atmospheric boundary layer: parameterizations of fluxes at the land surface require accurate data on soil and vegetation properties and states in combination with measurements of variables and fluxes in the atmospheric layer. This complete set of LAFO measurements will also be used to further develop dynamic plant growth photosynthesis models (Gayler et al., 2013, 2014). In addition, the LAFO site in-situ measurements facilitate straightforward comparison between measured and modelled time series of evapotranspiration, soil water content, soil temperature, soil matric potential, plant growth, plant development, leaf area index, yields, and the energy balance closure at the surface, all of which are considered important state variables to further develop the agroecological multi-model library Expert-N, and the land surface model NOAH-MP-GECROS. This further development is a prerequisite for coupling spatially explicit land surface models with large eddy simulations to account for field-to-field variability in crop/vegetation types and dynamics.

Further, we will use the WRF-NOAHMP model system, which includes plant dynamics components (GECROS model) and hydroecological components (HYDRO models). It can be used for both weather forecasts and climate simulations (Schwitalla and Wulfmeyer, 2014; Warrach-Sagi et al., 2013). The model already provides an ensemble of parameterizations, so that probabilistic investigations of their performance are also possible. Initial approaches to combining lidar data to analyse turbulence parameterizations were presented in Milovac et al. (2016). By combining different types of measurements as envisaged in LAFO, parameterizations can be determined much better and more reliably (Wulfmeyer et al., 2016).

2.2 Sensor Synergy

We have adopted a two-level observation strategy: long-term time series and IPOs. These provide us with parsimonious yet highly informative data sets obtained from our sensor synergy network.

On the long-term, we operate a number of instruments in operational mode to obtain continuous year-round time series. As such, since the beginning of LAFO in 2018, WaTSeN has been continuously supplying time series to characterize the spatial heterogeneity of soil water contents and temperatures at the Heidfeldhof. Similarly, two EC stations have been deployed. At the lidar site two Doppler lidars, a Doppler cloud radar, a micro rain radar and an optical distrometer have been continuously operated since May 2020. The vegetation status is registered on all plots with WaTSeN stations.

In addition to the operationally collected data, intensive observation periods will be organized as field experiments thereby complementing the operational instrumentation by additional sensors and measurement systems to get an almost full picture of the situation in the atmosphere, at the land surface, the vegetation and in the soil. This extended instrumentation is operated temporarily to target a certain aspect of L-A interaction. Additional instruments of UHOH are DIAL and RRL, BreedVision, Drones, EM38. Interesting sensors to add are further DLs for SL sampling, fibre-optical distributed sensing (FODS) to study the temperature distribution, canopy sensors to observe temperature, humidity, radiation, and wind inside and at the top of the canopy stand, and isotope measurements to discriminate between evaporation and transpiration. Interested external partners can benefit from our sensor synergy and join through collaboration. For example, LAFO was one observation site in the frame of the field campaign Swabian MOSES which took place in spring 2021 (Kunz et al., 2022). During this field experiment the Atmospheric Raman Temperature and Humidity Sounder (ARTHUS) was operated to capture atmospheric temperature and humidity profiles next to wind and cloud observations with DL and a Doppler cloud radar.

2.3 Study Area

LAFO site is located approximately 10 km south of Stuttgart city and 3km north from the Stuttgart airport, near the University of Hohenheim, Stuttgart (48° 42' N, 9°11' E) in Southwestern Germany. The study site belongs to the university's agricultural research farm "Heidfeldhof" and comprises 26 agricultural fields covering a surface area of 84 ha. Figure 2 shows a map of the LAFO study area. The agricultural fields are surrounded by suburban areas with an adjoining forest in the westerly direction. The Heidfeldhof farm is owned by the University of Hohenheim and used as a research site for agricultural experiments. Main crops are maize, rapeseed, wheat, triticale, and barley cultivated in rotation, which include other crops, too. The LAFO experimental site is flat; its elevation varies between 390 and 420 meters. The monthly temperatures vary between 0°C in winter and 18°C in summer months, and annual precipitation is 685 mm. An irrigation system is not installed. The soil type of the site is classified as Haplic Luvisol (periglacial loess) with a silty-loam texture (7 % sand, 73 % silt, and 21 % clay).

In addition to the LAFO measurements additional observations are made close by. In 2 km distance, the Hohenheim weather and climate station has been recording data since 1878. The meteorological observations at the Stuttgart airport (METAR code: ESSD) is located only 3 km to the South. The official weather station Stuttgart-Schnarrenberg operated by the German weather service (DWD) with radiosonde launches (two per day) is located 13 km to the Northwest. Finally, the water level of
230 the small Körsch creek next to the study area is recorded 8 km downstream to the East in Denkendorf.

3 Three LAFO components

The three LAFO components of the LAFO synergy are dedicated to the three compartments atmosphere, soil and land-surface, and vegetation and are described in the following and listed and located in Table 1 and Figure 2, respectively.

3.1 First LAFO component: Atmospheric measurements

235 The first component consists of three scanning lidar systems, a water vapor differential absorption lidar (DIAL), a water vapor and temperature rotational Raman lidar (RRL), and Doppler lidars (DLs) for wind measurements which are located at the lidar site (Figure 2). The DIAL and RRL have been developed and designed at the Institute of Physics and Meteorology of UHOH and the deployed Doppler lidars are manufactured by Halo Photonics Ltd. (UK). With this combination, it is possible to measure 2D to 3D structures of these important atmospheric variables from the ground through the boundary
240 layer to the lower free troposphere (about 3-4 km altitude). Particular, the coherent Doppler lidars are limited to regions with atmospheric scatters (aerosols, particles) which restricts the measurement range mostly to the ABL and thin clouds but have a nominal measurement range of 10 km. The range of DIAL and RRL reaches 5-6 km depending on the resolution. The DIAL is mounted on a mobile platform with a frequency-doubled Nd:YAG-pumed Ti:sapphire laser transmitter at 818 nm with an output power of up to 10 W (Wagner et al. 2013; Metzendorf, 2018). The 3D scanner is equipped with an 80-cm
245 primary mirror and allows scanning of the full upper hemisphere enabled for the first 3D humidity measurements (Späth et al., 2016). Raw signals are recorded with 0.1 s and 15 m and result in provided data resolutions of 1-10 s temporal and 60-300 m in range. The RRL is also a mobile, 3D scanning lidar system. The laser transmitter is based on a frequency tripled Nd:YAG laser at the eye-safe wavelength of 355 nm and a 40-cm receiving telescope with a 2-mirror 3D scanner (Radlach et al., 2008). A very efficient receiver separates the components of rotational Raman scattering for temperature and vibrational
250 Raman scattering for water vapor mixing ratio (WVMR) measurements (Hammann et al., 2015). Meanwhile, a more compact and automated Raman lidar for temperature and humidity measurements (Atmospheric Raman Temperature and HUmidity Sounder – ARTHUS, Lange et al., 2019) has been developed and is available at LAFO for collecting vertical profiles of temperature and humidity. The temporal and spatial resolutions are 1-10 s and 100-300 m. Wulfmeyer et al. (2015) demonstrated that the DIAL and the RRL are currently the most accurate and highest resolution water vapor and
255 temperature remote sensing systems in the world. The RRL was the first to measure inversions at the top of the boundary layer and turbulent fluctuations in daytime temperature (Behrendt et al., 2015). As research instruments, the scanning DIAL

and RRL are not automated, thus, manual operation is only affordable for certain time periods during dedicated intensive observations periods. Whereas ARTHUS is a full automated system to collect vertical profiles. When ARTHUS is not involved in other field campaigns, it is operated in LAFO.

260 The humidity and temperature measurements are complemented by wind measurements of two DLs which are operated continuously. One DL is dedicated to observe the vertical wind with turbulent resolving resolution of 1 s and 30 m in a constant vertical steering mode. The other DL is operated in 6-beam VAD (velocity azimuth display) mode to detect profiles of horizontal wind (Choukulkar et al, 2017). These measurements also have turbulence resolution with 90 s and 21 m. Wulfmeyer et al. (2016) showed that this measurement combination of DIAL, RRL, and DL is crucial for measuring fluxes

265 through the ABL and for developing new turbulence parameterizations. In combination with additional cross-track scanning DLs the measurement setup for SL profiling (Späth et al., 2016) can be achieved and used for mapping land surface fluxes. Additional instruments, e.g., DLs for cross-track scanning will be provided by project partners.

During cloudy and rainy weather situation one Doppler cloud radar (DCR) is operated in vertical stare mode. The DCR is a MIRA-36 of Metek GmbH (Görsdorf et al., 2015). The recorded DCR data has resolutions of 1 s and 30 m. To characterize

270 rain in more detail a micro rain radar (MRR, Metek GmbH) and an optical distrometer (ParSiVel) are installed as well. All instruments except DIAL and RRL are operated continuously and quicklooks of measurements are available in near real-time on the LAFO website https://lafo.uni-hohenheim.de/en.

3.2 Second LAFO component: soil and land-surface measurements

The second component combines sensors that determine energy fluxes at the land surface as well as state variables of soil.

275 Surface energy fluxes are derived from long-term eddy-covariance measurements at two stations at the Heidfeldhof (Figure 2). The stations are each fully equipped with a 3 m mast and sensors to measure CO_2/H_2O concentrations, 3D wind components with a sonic anemometer, and up-/downwelling shortwave (SW) and longwave (LW) radiation to access the net radiation Q_n. This instrumentation allows to investigate the energy partitioning of Q_n into sensible and latent surface heat fluxes S_0 and L_0, respectively, as well as ground heat flux G. All meteorological variables like air temperature, humidity,

280 pressure and precipitation are collected, as well as soil water content, soil temperature and matric potential at five soil depths (5, 15, 30, 45 and 75 cm) and averaged over 30 min time intervals. Variables to determine fluxes are recorded with 10 Hz and processed with TK3.1 (Mauder and Foken, 2015) resulting in 30-minutes values. The used sensors, characteristics, and methods are identical to Wizemann et al. (2015).

Beginning in June 2018 a Water and Temperature Sensor Network (WaTSeN) was installed to quantify the spatial-temporal

285 patterns of precipitation, soil water contents, and temperature with a total of 22 Aquaflex II universal sensors (Streat Instruments Ltd) to monitor the soil water content and temperature and 22 rain gauges (Pronamic) in November 2020, covering the entire Heidfeldhof (HFH; see Figure 2) area of 0.84 km^2. Aquaflex II sensors are installed below the ploughing depth in 40 cm depth providing year-round measurements without laborious sensor deinstallation. Rain gauges, solar panels, and loggers are mounted on a post next to each field. Stations are named according to site position and field site number with

the prefix "HFH". The stations are powered by solar electric panels. Each station is equipped with Adcon Remote Transmission Unit (RTU) data logger (OTT HydroMet GmbH) for automatically collecting and transmitting data via a 3G/4G network. Data loggers store sensor data taking the mean over 15-minute time intervals and data are then sent to the central database every six hours. Since factory calibrated volumetric water contents of Aquaflex II sensors are highly biased (Poltoradnev et al., 2015), the sensor signals are recalibrated based on site-specific soil sampling analysis. For this, soil core samples are systematically collected four times per year in close proximity to each soil sensor. The samples are used to determine the gravimetric water content by oven drying and converting them to volumetric water content by the determined bulk density. The determined values subsequently used for calibration of the Aquaflex II sensor data.

In Figure 3 the spatio-temporal variability of soil water content (SWC), its standard deviation and time series of precipitation for the two-year period 2019-2020 is shown. The SWC shows the typical wetting and drying cycles during the year reaching field capacity (the water content which can be held by capillary forces against gravity) in winter and subsequently long periods of drying between April and October as a result of net evapotranspiration being larger than precipitation over this period. SWC above field capacity are only observable during strong infiltration events and subsequent rapid drainage leads to plateaus in the observations, which is testimony to the high (un)saturated soil hydraulic conductivity. From the state-space of the standard deviation of SWC (σ_{SWC}) in Figure 3, we conclude that the variation in SWC is controlled by the land cover (through interception and absorption of plants and evaporation of soil) and by the fact that the infiltration fronts at 40-cm depth is far less homogenous (σ_{SWC} higher) than drying (σ_{SWC} lower).

So far, we have not detected strong coupling between the soil hydrological variables and fluxes at the land surface during the growing seasons. Latent and sensible heat fluxes show no significant correlation with SWC or water potential in any depths. Thus far, soil variables have not been shown to control the fluxes at the land surface during the growing season, and heat fluxes are radiation driven. This can be beneficial since it allows to identify the plant state as the principal control for spatial surface flux heterogeneity at the land surface.

3.3 Third LAFO component: vegetation measurements

This component consists of equipment for characterizing vegetation. These include UAVs for recording plant characteristics, which now represent an innovative alternative to traditional remote sensing with manned aircraft or satellites due to the inexpensive and short-term availability of high-spatial-resolution sensor data. Especially the higher spatial resolution allows applications on smaller field plots. For the determination of vegetation indices for the derivation of biomass and nitrogen supply, several spectral bands are necessary (e.g. 670, 700, 740 and 780 nm) for the calculation of the Red Edge Inflection Point (REIP). The spectral analysis was performed with a UAV equipped with converted industrial 4-sensor camera for REIP imaging by means of suitable interference filters (Geipel et al., 2014). In addition, the camera has been coupled to an external light meter to dynamically adjust the exposure time to the solar irradiance. The camera is individually programmable and also allows image processing in near real-time.

In cooperation with the Osnabrück University of Applied Sciences, the State Seed Breeding Institute (LSA) at the UHOH has developed the "BreedVision" phenotyping platform (Busemeyer et al., 2013). It consists of a carrier vehicle and a sensor module. The carrier vehicle is a high-wheel tractor especially adapted to the requirements of the sensor module. Both the track width and the height of the carrier vehicle can be adjusted hydraulically. The sensor module includes sensors with different morphological or spectral selectivity such as light grids, laser distance sensors, multi-reflective ultrasonic sensors, digital cameras, a plenoptic camera, and a hyperspectral camera. For example, light grids create a shadow image from the transmitted light through the plants of the plots, from which plant height z_p and density can be indirectly determined, while a hyperspectral camera can be used to determine plant moisture content or parameters such as the normalized differential vegetation index (NDVI). The sensor module is continuously adjustable in height, allowing a constant distance of the sensors to the plants, even with varying plant heights. The particularly innovative feature of the developed system is the combination of sensor data for trait prediction. The spatial and temporal allocation of all sensor data to a single position and thus to individual plant organs in the crop, which is necessary for this, is so far unique in field phenotyping. In addition to its use in plant breeding, the system can also be used to record, by means of the various complementary sensors, a range of trait parameters along a plant stand.

Further, we routinely register the leaf-area index (LAI) with a LAI2200C sensor from LI-COR Biosciences Inc. (USA), the crop height and phenomenological growth stage using the BBCH code (Biologische Bundesanstalt für Land- und Forstwirtschaft, Bundessortenamt und Chemische Industrie; Meier, 2018) at our EC and WaTSeN stations throughout the main vegetation period (biweekly). Furthermore, we have a set of canopy sensors to investigate temperature and humidity at different levels inside and right above the canopy top.

4 Measurement examples

The LAFO equipment and its data products are listed in Table 1. The list contains the currently operationally available instruments and measurement data but can be extended in the future or for measurement campaigns with collaborators complementing instrumentation for certain time periods.

4.1 Dynamic and thermodynamic profiling for turbulence analysis

For studying dynamics and thermodynamics in the ABL at LAFO we use the synergy of DLs and ARTHUS. As explained in Sect. 2.2, we measure dynamic profiles of vertical wind with one constantly vertical pointing DL and retrieve the horizontal wind from DL in 6-beam VAD mode. In Figure 4 we show 24-hour wind measurements for 27 June 2021. The figure shows in (A)-(D) vertical profiles of vertical and horizontal wind as well as profiles of the backscatter coefficient. The resolution of the vertical wind and backscatter coefficient is 1 s and 30 m. The horizontal wind is retrieved from the 6-beam VAD mode with a sinusoidal fit and results in a 90 s and 21 m temporal and spatial resolution (Bonin et al., 2017). To reduce the effect of the convective eddies for the horizontal wind, an additional gliding average of 21 minutes was applied. In the vertical

wind plot (A) the development of the CBL started around 07 UTC which is indicated by the stronger up and down draft starting to grow from the surface into the boundary layer. The CBL stayed convective until around 17 UTC and reached a

355 height of around 1 km. Before and after that period only low vertical wind was observed which is typical for the night time boundary layer. While there was nearly no vertical motion at the beginning of the day a low-level jet (LLJ) in the horizontal wind up to 8 ms^{-1} was recorded at a height of 500 m. This LLJ disappeared at around 10 UTC when the convective motion reached the height of the LLJ. Recording the data with turbulence resolution allows the derivation of further products like vertical wind variance, momentum flux and turbulent kinetic energy which are plotted in (E)-(G). For these retrievals we

360 determine the fluctuations to calculate the variance and higher-order moments (not shown here) following the method of Lenschow et al. (2000) and Wulfmeyer et al. (2016). This method also allows to distinguish between atmospheric variance and instrumental noise contribution. The calculation of momentum flux and TKE follows Bonin et al. (2017). In the evening at 20 and 23 UTC two rain events were captured which are identified by reduced measurements range or strong downward motion and corresponding effects in the derived products.

365 The thermodynamic profiling was performed with ARTHUS. The time series of WVMR and temperature profiles of 27 June 2021 are shown in Figure 5 (A) and (B). The data show the moistening and warming of boundary layer in the cause of the day when the boundary layer became convective. In combination with vertical wind measurements the latent and sensible heat fluxes through the boundary layer can be calculated with the covariances of humidity and temperature fluctuations and vertical wind (Behrendt et al., 2020) and are plotted in Figure 5 (C) and (D). When including horizontal wind, the water

370 vapor budget in the BL can be determined as demonstrated for the first time for a LAFE case by Lange et al. (2022). This measurement synergy demonstrates the atmospheric link for the investigation of energy and water budget as aimed in LAFO objective 1.

4.2 Correlation between turbulent mixing height and surface fluxes

With the wind observation the turbulent motion in the BL can be captured. The depth of the CBL is related to the energy

375 intake by solar radiation and its partitioning at the land surface. Thus, we determined the mixing height for the three-month period from 01 May to 31 July 2021 and correlate them to the surface fluxes measured with the EC station.

For determining the mixing layer height (MLH) we use vertically pointing Doppler lidar and Doppler cloud radar data and a fuzzy logic approach to weight the different data (Bonin et al., 2018). The DL measures the vertical wind w, signal-to-noise ratio (SNR) and backscatter coefficient β and from the DCR vertical profiles of radar reflectivity, Doppler velocity and

380 spectral width are included in the algorithm. The main contribution comes from the vertical wind variance to map variance as turbulent for $<w'^2> \geq 0.1$ m^{2}s^{-2} or non-turbulent. A SNR threshold was set to filter the wind data for poor data quality and high β values are used as indicator for the presence of clouds and precipitation. Clouds show high β values and a strong β gradients at the cloud bottom and precipitation is associated with high β values and negative vertical wind. In addition, the

DCR data are used to support cloud and precipitation estimates. Data of clouds and precipitation are filtered out and are not included in the determination of MLH.

The MLH is calculated for each day for the time period between 06:00 and 18:00 UTC which covers daytime between sunrise and sunset when turbulent mixing is expected. The analysis is based on the 1 s data. Night-time MLH usually is very low and mixing is caused by friction between air and land surface. These situations cannot be captured with our vertical pointing instruments as the lowest range bin is not lower than 100 m. Data of the 1 s MLH data are averaged for 30-minute intervals as the surface fluxes are calculated likewise for half-hour timeslots. In Figure 6 (A) the statistics of the diurnal cycle of the MLH is plotted as whisker box plot. The box and whiskers provide a clear picture of data distribution. The box itself represents the range of 50 % central data (between 25 % and 75 %) also known as interquartile range (IQR). In the box the red line gives the median of the data. The dashed lines (whiskers) extending from the box marking the remaining data ranging from the minimum to the maximum values. Data points outside of these ranges are considered as outliers which is defined as < 1.5 IQR or > 1.5 IQR. The dashed curve and red dots follow the mean MLH. For the surface fluxes of sensible and latent heat and of the net radiation for the 30-minutes intervals also the whisker box plots are shown in Figure 6 (B)-(D). The correlation of the mean MLH and the fluxes was plotted in Figure 7.

The statistics include the full three-month period covering all cases including clear sky, clouds, rain, and thunderstorms. On convective days the MLH reached in the mean up to around 1.2 km and over all up to more than 2 km, however, on cloudy days the MLH stays about 400 m lower. This is also represented in the flux data when on cloudy days the surface heating is low. The sensible heat flux varies from 20 to 70 Wm^{-2}, latent heat flux varies from 20 to 300 Wm^{-2}, and net radiation from 20 to 400 Wm^{-2}. The growing of the MLH starts in the morning when convection starts with the surface heating after sunrise and decays when the energy input decreases. Thus, MLH development is clearly related to the surface fluxes. The maximum is reached around noon when most energy is available. This is also reflected by the positive correlation of the mean MLH and the surface fluxes plotted in Figure 7. The MLH is directly correlated with sensible heat flux and net radiation whereas the correlation to latent heat flux shows a hysteresis effect. The growing MLH follows the increasing latent heat flux but the MLH decays in the afternoon even when the latent heat flux is still present and does not decrease with a similar rate.

This example illustrated to use of long-term dataset to evaluate statistics and relationships between variables of different compartments like atmosphere and land-surface. Such relationships are the first step to develop new parameterizations or metrics for the description in land-surface models or to test existing models as we strive for in LAFO objective 3.

4.3 Scanning lidar observations

To observe the direct link between atmosphere and land surface we make use of the scanning capability of our lidar instruments. With low elevation scanning lidar measurements we are able to observe surface layer profiles of horizontal wind, humidity content, and temperature (Späth et al., 2022). Figure 8 demonstrates humidity measurements with the scanning WV DIAL across the agricultural fields to the north-western direction. The scan direction and a photograph are shown in Figure 8 (A). For the measurement the lidar scanning unit (Figure 8 (A)) moved with $0.2°s^{-1}$ for a 90° angle range

and the data were analysed with 10 s and 67.5 m temporal and spatial resolutions, respectively. The measurement was performed on 20 October 2020 at 14:16 UTC. The plot in Figure 8 (B) shows four layers in the lowest 0.5 km of which the highest WV content is found in the lowest layer close to the ground and decreasing humidity content in the layers above. The lowest layer shows spatial variations along the scan axis with a lower humidity content at 500 to 600 m and an increase at 650 m. It is noteworthy that the high resolution of the WV DIAL measurement to be as sensitive as to resolve variabilities of less than 1 gm^{-3}. As the atmosphere is moistening from the surface, we can relate the structures close to the surface to land-surface properties as explained by Späth et al. (2016). Being already in autumn and most of the fields were harvested we make use of the WaTSeN stations. Here we measure the water content of the soil as indication for the potential of evaporation and transpiration at the land-surface. In Figure 8 (C) the soil water content of the WaTSeN stations HFH 1-9 is given with respect to the distance to the WVDIAL. The course of the soil water content in Figure 8 (C) shows a minimum at 550 m distance and a maximum of water content at 700 m. This agrees with the behaviour of the atmospheric humidity observed with the lidar in the atmosphere above.

In the region with low atmospheric humidity below was intertillage on the fields in a small growing stage. Closer and farer the fields were bare soil where higher evaporation is enabled according to higher soil water content. This observation displays how heterogenic landscape and corresponding atmospheric structures can be observed with scanning lidars and the soil sensor network within the LAFO instrumentation. This kind of observations allow to work on LAFO objective 2 regarding surface fluxes in heterogeneous terrain.

5 Summary and Outlook

Important topics in L-A feedback research are water and energy balances and heterogeneities of fluxes at the land-surface and in the ABL. To target these questions, the land-atmosphere feedback observatory LAFO has been installed as first GEWEX LAFO. LAFO is dedicated for L-A feedback research located in Southwest Germany in mid-latitude continental climate and demonstrates the GLASS panel proposed instrumentation allowing comprehensive and high-resolution measurements from the bedrock to the lower free troposphere. Grouped in three components: atmosphere, soil and land-surface and vegetation, the LAFO observation strategy aims for simultaneous measurements in all three compartments. For that, the LAFO sensor synergy contains lidar systems to measure the atmospheric key variables humidity, temperature and wind. At the land-surface two EC station are operated to record the energy distribution of radiation, sensible, latent and ground heat fluxes. In the soil under the EC stations profiles of soil water content, soil temperature and matric potential are measured. With WaTSeN the soil water and temperature are monitored in the agricultural investigation area. The vegetation status is registered by crop height and LAI measurements, and phenological growth stage (BBCH).

The observations in LAFO are organized in operational measurements and intensive observations periods (IOPs). Operational measurements aim for long time-series dataset to investigate statistics like the demonstrated correlation between MLH and surface fluxes. Furthermore, the long-term dataset from the EC stations are interesting to be used for machine

learning approaches to investigate new SL relationships as demonstrated by Wulfmeyer et al. (2022b). During IOPs non-automated instruments complements the operational instrumentation for extended analysis like analysis of sensible and latent heat fluxes in the ABL with humidity and temperature measurements from ARTHUS or SL observations of humidity with the scanning capability of the WV DIAL to relate atmospheric moisture distribution to soil water structures. The three measurement examples illustrate how the LAFO instrumentation will be used to target the three LAFO objectives to investigate LA feedback.

Further, some of LAFO's measurement technology has significant commercialization potential. In particular, the development of compact and operational water vapor and temperature profilers (ARTHUS, Lange et al., 2019; NCAR DIAL, Spuler et al., 2015) with high resolution and accuracy has long been requested for use in national and international networks to improve weather forecasting (Adam et al., 2016; Weckwerth et al., 2016; Thundathil et al., 2020, 2021), climate monitoring, verification of models and satellite measurements, and data assimilation. LAFO can serve as a platform to test and develop new devices of this kind and support the GLASS panel vison to setup GLAFOs in all climate regions.

In the upcoming months and years, not only will the observational dataset continuously grow but also be made publicly available. Our database is based on the open-source available data portal software of TEODOOR (Kunkel et al., 2013) and connected to the European Network of Hydrological Observatories (enoha, https://enoha.eu/) and allows access to and visualization of quality controlled timeseries of EC station data and of the WaTSeN data. Later also 2D dataset from the DLs and the DCR will be accessible. Until then, near real-time time-height cross-section plots of DL and DCR data are available on the LAFO website (http://lafo.uni-hohenheim.de/en). In addition to the observations, model runs of large eddy simulation will be prepared for the LAFO region and performed with different configurations of the Weather Research and Forecast (WRF) model (Bauer et al., 2022). With respect to model efforts, LAFO data can be used for model evaluation, process studies or data assimilation ideas.

6 Data availability

The presented data will be made publicly available with acceptance of the manuscript. Until then, data are available on request to the corresponding authors. All raw data can be provided by the corresponding authors upon request.

7 Author contribution

VW, AB and TS designed the observation strategy and FS, VR, TKDW, SM, JI, DL carried them out. FS, VR, TKDW, SM, DL, and SSA analysed the data. FS, VR, TKDW prepared the manuscript with contributions from all co-authors

8 Competing interests

The authors declare that they have no conflict of interest.

9 Acknowledgment

We thank the Carl Zeiss Foundation for funding the setup phase of LAFO as part of its program to strengthen research
480 infrastructures at universities. Further, we kindly thank Herbert Stelz, Stefan Pilz, Timo Keller, Thomas Schreiber, Christian Schade and Jacky Schulz for their different levels of support and measurements.

References

Adam, S., Behrendt, A., Schwitalla, T., Hammann, E. and Wulfmeyer, V.: First assimilation of temperature lidar data into a numerical weather prediction model: Impact on the simulation of the temperature field, inversion strength, and planetary
485 boundary layer depth. Q. J. Roy. Meteor. Soc. 142 (700), 2882-2896, doi:10.1002/qj.2875, 2016.

Anderegg, W. R. L., Anderegg, L. D. L., Kerr, K. L., Trugman, A. T.: Widespread drought-induced tree mortality at dry range edges indicates that climate stress exceeds species' compensating mechanisms, Global Change Biology, 25, 11, 3793-3802, doi:10.1111/gcb.14771, 2019.

Baldocchi, D., Falge, E., Gu, L., Olson, R., Hollinger, D., Running, S., Anthoni, P., Bernhofer, Ch., Davis, K., Evans, R.,
490 Fuentes, J., Goldstein, A., Katul, G., Law, B., Lee, X., Malhi, Y., Meyers, T., Munger, W., Oechel, W., Paw U, K. T., Pilegaard, K., Schmid, H. P., Valentini, R., Verma, S., Vesala, T., Wilson, K., & Wofsy, S.: FLUXNET: A New Tool to Study the Temporal and Spatial Variability of Ecosystem-Scale Carbon Dioxide, Water Vapor, and Energy Flux Densities, Bulletin of the American Meteorological Society, 82(11), 2415-2434, doi:10.1175/1520-0477(2001)082<2415:FANTTS>2.3.CO;2, 2001.

495 Bauer, H.-S., Späth, F., Lange, D., Senff, C., Thundathil, R., Ingwersen, J., Salami, D.T., Behrendt, A., Wulfmeyer, V.: Nested WRF simulations down to the turbulence-permitting scale for a cloud-free case during the LAFE campaign in August 2017. Evolution of the convective boundary layer compared to observations, Journal of Geophysical Research: Atmospheres, submitted, 2022.

Behrendt, A., Wulfmeyer, V., Hammann, E., Muppa, S. K., and Pal, S.: Profiles of second- to fourth-order moments of
500 turbulent temperature fluctuations in the convective boundary layer: first measurements with rotational Raman lidar. Atmos. Chem. Phys. 15, 5485-5500, doi:10.5194/acp-15-5485-2015, 2015.

Behrendt, A., Wulfmeyer, V., Senff, C., Muppa, S. K., Späth, F., Lange, D., Kalthoff, N., and Wieser, A.: Observation of sensible and latent heat flux profiles with lidar. Atmos. Meas. Tech. 13, 3221-3233, doi:10.5194/amt-13-3221-2020, 2020.

505 Betts, R. A., Cox, P. M., Collins, M., Harris, P. P., Huntingford, C. and Jones, C. D.: The role of ecosystem-atmosphere interactions in simulated Amazonian precipitation decrease and forest dieback under global climate warming. Theor. Appl. Climatol. 78, 157–175 (2004), doi: 10.1007/s00704-004-0050-y, 2004.

Betts, R. A., Boucher, O., Collins, M., Cox, P. M., Falloon, P. D., Gedney, N., Hemming, D. L., Huntingford, C., Jones, C. D., Sexton, D. M. H. and Webb, M. J.: Projected increase in continental runoff due to plant responses to increasing carbon dioxide, Nature, 448,1037–1041, doi:10.1038/nature06045, 2007.

Bonin, T. A., Choukulkar, A., Brewer, W. A., Sandberg, S. P., Weickmann, A. M., Pichugina, Y. L., Banta R. M., Oncley, S. P., and Wolfe, D. E.: Evaluation of turbulence measurement techniques from a single Doppler lidar, Atmos. Meas. Tech., 10, 3021–3039, doi:10.5194/amt-10-3021-2017, 2017.

Bonin, T. A., Carroll, B. J., Hardesty, R. M., Brewer, W. A., Hajny, K., Salmon, O. E., and Shepson, P. B.: Doppler Lidar Observations of the Mixing Height in Indianapolis Using an Automated Composite Fuzzy Logic Approach, Journal of Atmospheric and Oceanic Technology, 35(3), 473-490, doi:10.1175/JTECH-D-17-0159.1, 2018.

Branch, O., and Wulfmeyer, V.: Deliberate enhancement of rainfall using desert plantations. P. Natl. Acad. Sci. USA. 116(40), 18841-8847, doi: 10.1073/pnas.1915645116, 2019.

Busemeyer, L., Mentrup, D., Möller, K., Wunder, E., Alheit, K., Hahn, V., Maurer, H.P., Reif, J.C., Würschum, T., Müller, J., Rahe, F., Ruckelshausen, A.: BreedVision - A Multi-Sensor Platform for Non-Destructive Field-Based Phenotyping in Plant Breeding. Sensors, 13, 2830-2847, doi:10.3390/s130302830, 2013.

Chen, L., and Dirmeyer, P.A.: Impacts of land-use/land-cover change on afternoon precipitation over North America. J. Climate 30, 2121-2140, doi:10.1175/JCLI-D-16-0589.1, 2017.

Choukulkar, A., Brewer, W. A., Sandberg, S. P., Weickmann, A., Bonin, T. A., Hardesty, R. M., Lundquist, J. K., Delgado, R., Iungo, G. V., Ashton, R., Debnath, M., Bianco, L., Wilczak, J. M., Oncley, S., and Wolfe, D.: Evaluation of single and multiple Doppler lidar techniques to measure complex flow during the XPIA field campaign Atmos. Meas. Tech., 10, 247–264, doi:10.5194/amt-10-247-2017, 2017.

Davin, E.L., Seneviratne, S.I., Ciais, P., Olioso, A., and Wang, T.: Preferential cooling of hot extremes from cropland albedo management. P. Natl. Acad. Sci. 111, 9757–9761, doi:pnas.1317323111, 2014.

Davin, E.L., Rechid, D., Breil, M., Cardoso, R.M., Coppola, E., Hoffman, P., Jach, L.L., Katragkou, E., de Noblet-Ducoudré, N., Radke, K., Raffa, M., Soares, P.M.M., Sofiadis, G., Strada, S., Strandberg, G., Tölle, M.H., Warrach-Sagi, K., and Wulfmeyer, V.: Biogeophysical impacts of forestation in Europe: First results from the LUCAS Regional Climate Model intercomparison. Earth Syst. Dynam. 11, 183–200, doi:10.5194/esd-11-183-2020, 2020.

Devanand, A., Huang, M., Lawrence, D.M., Zarzycki, C.M., Feng, Z., Lawrence, P.J., Qian, Y., and Yang, Z.: Land use and land cover change strongly modulates land-atmosphere coupling and warm-season precipitation over the central United States in CESM2-VR. J. Adv. Model. Earth Sy. 12, e2019MS001925, DOI:10.1029/2019MS001925, 2020.

Dirmeyer, P.A., Cash, B.A., Kinter Ill, J.L., Stan, C., Jung, T., Marx, L., Towers, P., Wedi, N., Adams, J.M., Altshuler, E.L., Huang, B., Jin, E.K., and Manganello, J.: Evidence for enhanced land–atmosphere feedback in a warming climate. *J. Hydrometeorol.* 13(3), 981-995, DOI:10.1175/JHM-D-11-0104.1, 2012.

Dirmeyer, P. A., Chen, L., Wu, J., Shin, C., Huang, B., Cash, B. A., Bosilovich, M. G., Mahanama, S., Koster, R. D., Santanello, J. A., Ek, M. B., Balsamo, G., Dutra, E., & Lawrence, D. M., Verification of Land–Atmosphere Coupling in

Forecast Models, Reanalyses, and Land Surface Models Using Flux Site Observations, *J. Hydrometeorol.*, *19*(2), 375-392, doi:10.1175/JHM-D-17-0152.1, 2018.

Dirmeyer, P.A., The cusp of major progress in predicting land-atmosphere interactions, GEWEX News 24(1-2), 15-18, 2014.

Ek, M., and Holtslag, A.A.M.: Influence of soil moisture on boundary layer cloud development. *J. Hydrometeorol.* 5(1), 86-99, DOI:10.1175/1525-7541(2004)005<0086:IOSMOB>2.0.CO;2, 2004.

Franz, D. et al.: Towards long-term standardised carbon and greenhouse gas observations for monitoring Europe´s terrestrial ecosystems: a review, Int. Agrophys., 32, 439-455, doi:10.1515/intag-2017-0039, 2018.

Gayler, S., Ingwersen, J., Priesack, E., Wöhling, T., Wulfmeyer, V., and Streck, T.: Assessing the relevance of sub surface processes for the simulation of evapotranspiration and soil moisture dynamics with CLM3.5: Comparison with field data and crop model simulations, Environ. Earth Sci., 69(2), 415–427, doi:10.1007/s12665-013-2309-z, 2013.

Gayler, S., Wöhling, T., Grzeschik, M., Ingwersen J., Wizemann, H.-D., Warrach-Sagi, K., Högy, P., Attinger, S., Streck, T., and Wulfmeyer, V.: Incorporating dynamic root growth enhances the performance of Noah-MP ensemble simulations at two contrasting winter wheat field sites. Water Resour. Res. 50(2), 1337-1356, doi:10.1002/2013WR014634, 2014.

Geipel, J.; Link, J.; Claupein, W.: Combined Spectral and Spatial Modeling of Corn Yield Based on Aerial Images and Crop Surface Models Acquired with an Unmanned Aircraft System. Remote Sens., 6, 10335-10355, doi:10.3390/rs61110335, 2014.

Gentine, P., Holtslag, A. A. M., D'Andrea, F., and Ek, M.: Surface and Atmospheric Controls on the Onset of Moist Convection over Land, Journal of Hydrometeorology, 14(5), 1443-1462, doi:10.1175/JHM-D-12-0137.1, 2013.

Hammann, E., Behrendt, A., Le Mounier, F., and Wulfmeyer, V.: Temperature profiling of the atmospheric boundary layer with rotational Raman lidar during the HD(CP)2 Observational Prototype Experiment. Atmos. Chem. Phys. 15, 2867-2881, doi: 10.5194/acp-15-2867-2015, 2015.

Helbig, M., Gerken, T., Beamesderfer, E.R., Baldocchi, D.D., Banerjee, T., Biraud, S.C., Brown, W.O.J., Brunsell, N.A., Burakowski, E.A., Burns, S.P., Butterworth, B.J., Chan, W.S., Davis, K.J., Desai, A.R., Fuentes, J.D., Hollinger, D.Y., Kljun, N., Mauder, M., Novick, K.A., Perkins, J.M., Rahn, D.A., Rey-Sanchez, C., Santanello, J.A., Scott, R.L., Seyednasrollah, B., Stoy, P.C., Sullvan, R.C., Vilà-Guerau de Arellano, J., Wharton, S., Yi, C., and Richardson, A.D.: Integrating continuous atmospheric boundary layer and tower-based flux measurements to advance understanding of land-atmosphere interaction. Agr. Forest Meteorol. 307, 108509, DOI:10.1016/j.agrformet.2021.108509, 2021.

Holt, T.R., Niyogi, D., Chen, F., Manning, K., LeMone, M.A., and Qureshi, A.: Effect of land–atmosphere interactions on the IHOP 24–25 May 2002 convection case. Mon. Weather Rev. 134, 113-133, DOI:10.1175/MWR3057.1, 2006.

Imukova, K., Ingwersen, J., Hevart, M., and Streck, T.: Energy balance closure on a winter wheat stand: Comparing the eddy covariance technique with the soil water balance method. Biogeosciences 13, 63–75, DOI:10.5194/bg-13-63-2016, 2016.

Ingwersen, J., Imukova, K., Högy, P., and Streck, T.: On the use of the post-closure methods uncertainty band to evaluate the performance of land surface models against eddy covariance flux data. Biogeosciences 12, 2311–2326, DOI:10.5194/bg-12-2311-2015, 2015.

IPCC, [V. Masson-Delmotte, P. Zhai, A. Pirani, S. L. Connors, C. Péan, S. Berger, N. Caud, Y. Chen, L. Goldfarb, M. I. Gomis, M. Huang, K. Leitzell, E. Lonnoy, J.B.R. Matthews, T. K. Maycock, T. Waterfield, O. Yelekçi, R. Yu and B. Zhou], 2021: Summary for Policymakers. In: Climate Change 2021: The Physical Science Basis. Contribution of Working Group I to the Sixth Assessment Report of the Intergovernmental Panel on Climate Change. Cambridge University Press, In Press, [online], https://www.ipcc.ch/report/ar6/wg1/downloads/report/IPCC_AR6_WGI_SPM.pdf

Jacob, D., Teichmann, C., Sobolowski, S., Katragkou, E., Anders, I., Belda, M., Benestad, R., Bobern, F., Buonomo, E., Cardoso, R.M., Casanueva, A., Christensen, O.B., Hesselbjerg Christensen, J., Coppola, E., De Cruz, L., Davin, E.L., Dobler, A., Domínguez, M., Fealy, R., Fernandez, J., Gaertner, M.A., Garcia-Díez, M., Giorgi, F., Gobiet, A., Goergen, K., Gómez-Navarro, J.J., González Alemán, J.J., Gutiérrez, C., Gutiérrez, J.M., Güttler, I., Haensler, A., Halenka, T., Jerez, S., Jiménez-Guerrero, P., Jones, R.G., Keuler, K., Kjellström, E., Knist S., Kotlarski, S., Maraun, D., van Meijgaard, E., Mercogliano, P., Montávez, J.P., Navarra, A., Nikulin, G., de Noblet-Ducoudré, N., Panitz, H.-J., Pfeifer, S., Piazza, M., Pichellli, E., Pietikäinen, J.-P., Prein, A.F., Preuschmann, S., Rechid, D., Rockel, B., Romera, R., Sánchez, E., Sieck, K., Soares, P.M.M., Somot, S., Srnec, L., Lund Sørland, S., Termonia, P., Truhetz, H., Vautard, R., Warrach-Sagi, K., and Wulfmeyer, V.: Regional climate downscaling over Europe: perspectives from the EURO-CORDEX community. Reg. Environ. Change 20, 51, DOI:10.1007/s10113-020-01606-9, 2020.

Jaeger, E.B., and Seneviratne, S.I.: Impact of soil moisture–atmosphere coupling on European climate extremes and trends in a regional climate model. Clim. Dynam. 36, 1919–1939, DOI:10.1007/s00382-010-0780-8, 2011.

Kunkel, R., Sorg, J., Eckardt, R., Kolditz, O., Rink, K., Vereecken, H., TEODOOR: a distributed geodata infrastructure for terrestrial observation data, Environ. Earth Sci. 69:507-521, doi:10.1007/s12665-013-2370-7, 2013

Kunz, M., Abbas S.S., Bauckholt, M., Böhmländer, A., Feuerle, T., Gasch, P., Glaser, C., Groß, J., Hajnsek, I., Handwerker, J., Hase, F., Khordakova, D., Knippertz, P., Kohler, M., Lange, D., Latt, M., Laube, J., Martin, L., Mauder, M., Möhler, O., Mohr, S., Reitter, R.W., Rettenmeier, A., Rolf, C., Saathoff, H., Schrön, M., Schütze, C., Spahr, S., Späth, F., Vogel, F., Völksch, I., Weber, U., Wieser, A., Wilhelm, J., Zhang, H. and Dietrich, P., Swabian MOSES 2021: An interdisciplinary field campaign for investigating convective storms and their event chains, Front. Earth Sci. 10:999593, doi:10.3389/feart.2022.999593, 2022.

Lange, D., Behrendt, A., and Wulfmeyer, V.: Compact operational tropospheric water vapor and temperature Raman Lidar with turbulence resolution. Geophys. Res. Lett., 46(24), 14844-14853, doi:10.1029/2019GL085774, 2019.

Lange D., Behrendt, A., Senff, C., Späth, F., Turner, D.D., Wulfmeyer, V.: Water vapor budget during LAFE field campaign, in preparation, 2022.

Lee, T. R. and Buban, M.: Evaluation of Monin–Obukhov and Bulk Richardson Parameterizations for Surface–Atmosphere Exchange, Journal of Applied Meteorology and Climatology, 59(6), 1091-1107, DOI:10.1175/JAMC-D-19-0057.1, 2020.

Lee, T., Buban, M., Dumas, E., and Baker, C.: On the Use of Rotary-Wing Aircraft to Sample Near-Surface Thermodynamic Fields: Results from Recent Field Campaigns, Sensors, 19(1), 10, doi:10.3390/s19010010, 2019.

Lenschow, D. H., Wulfmeyer, V., and Senff, C.: Measuring second-through fourth-order moments in noisy data. J. Atmos. Oceanic Tech. 17(10), 1330-1347, doi:10.1175/1520-0426(2000)017<1330:MSTFOM>2.0.CO;2, 2000.

Mauder, M. and Foken, T.: Documentation and Instruction Manual of the Eddy-Covariance Software Package TK3 (update), Arbeitsergebnisse, University of Bayreuth, Bayreuth, 62 pp., 2015.

Mauder, M., Foken, T., and Cuxart, J.: Surface-Energy-Balance Closure over Land: A Review, Bound.-Lay. Meteor., 177, 395–426, doi:10.1007/s10546-020-00529-6, 2020.

McDermid, S.S., Montes, C., Cook, B.I., Puma, M.J., Kiang, N.Y., and Aleinov, I.: The sensitivity of land–atmosphere coupling to modern agriculture in the Northern Midlatitudes. J. Climate 32(2), 465-484, DOI:10.1175/JCLI-D-17-0799.1, 2019.

Meier, U.: Growth stages of mono- and dicotyledonous plants: BBCH Monograph, Open Agrar Repositorium, Julius Kühn-Institut (JKI), Quedlinburg, Germany, 2018.

Metzendorf, S.: 10 W-Average-Power single-frequency Ti:sapphire Laser with tuning agility – A breakthrough in high-resolution 3D water-vapor measurement. Dissertation, University of Hohenheim, Institute for Physics and Meteorology, http://opus.uni-hohenheim.de/volltexte/2019/1558/, 2018.

Milovac, J., Warrach-Sagi, K., Behrendt, A., Späth, F., Ingwersen, J., and Wulfmeyer, V.: Investigation of PBL schemes combining the WRF model simulations with scanning water vapor differential absorption lidar measurements. J. Geophys. Res.- Atmos. 121(2), 624-649, doi: 10.1002/2015JD023927, 2016.

Miralles, D., Teuling, A., van Heerwaarden, C.C., and Vilà-Guerau de Arellano, J.: Mega-heatwave temperatures due to combined soil desiccation and atmospheric heat accumulation. Nature Geosci. 7, 345–349, DOI:10.1038/ngeo2141, 2014.

Miralles, D.G., Gentine, P., Seneviratne, S.I., and Teuling, A.J.: Land-atmospheric feedbacks during droughts and heatwaves: state of the science and current challenges. Ann. NY Acad. Sci. 1436(1), 19-35, DOI:10.1111/nyas.13912, 2019.

Muppa, S. K., Behrendt, A., Späth, F., Wulfmeyer, V., Metzendorf, S., and Riede, A.: Turbulent humidity fluctuations in the convective boundary layer: Case studies using water vapour differential absorption lidar measurements. Bound.-Lay. Meterorol. 158, 43-66, doi:10.1007/s10546-015-0078-9, 2016.

Nolan, C., Overpeck, J.T., Allen, J.R.M., Anderson, P.M., Betancourt, J.L., Binney, H.A., Brewer, S., Bush, M.B., Chase, B.M., Cheddadi, R., Djamali, M., Dodson, J., Edwards, M.E., Gosling, W.D., Haberle, S., Hotchkiss, S.C., Huntley, B., Ivory, S.J., Kershaw, A.P., Kim, S.-H., Latorre, C., Leydet, M., Lézine, A.-M., Liu, K.-B., Liu, Y., Lothkin, A.V.,

640 McGlone, M.S., Marchanz, R.A., Momohara, A., Moreno, P.I., Müller, S., Otto-Bliesner, B.L., Shen, C., Stevenson, J., Takahara, H., Tarasov, P.E., Tipton, J., Vincens, A., Weng, C., Xu, Q., Zheng, Z., and Jackson, S.T.: Past and future global transformation of terrestrial ecosystems under climate change. Science 361, 920-923, DOI:10.1126/science.aan5360, 2018.

Novick, K.A., Biederman, J.A., Desai, A.R., Litvak, M.E., Moore, D.J.P., Scott, R.L., Torn, M.S.: The AmeriFlux network:
645 A coalition of the willing, Agricultural and Forest Meteorology, 249, 444-456, doi:10.1016/j.agrformet.2017.10.009, 2018.

Pearson, G., Davies, F., and Collier, C.: An Analysis of the Performance of the UFAM Pulsed Doppler Lidar for Observing the Boundary Layer. J. Atmos. Ocean. Technol. 26, 240–250, doi:10.1175/2008JTECHA1128, 2009.

Poltoradnev M., Ingwersen J., Streck T.: Calibration and Application of Aquaflex TDT Soil Water Probes to Measure the
650 Soil Water Dynamics of Agricultural Topsoil in Southwest Germany. Journal of Irrigation and Drainage Engineering, 141: 04014072. doi: 10.1061/(asce)ir.1943-4774.0000838., 2015.

Radlach, M., Behrendt, A., and Wulfmeyer, V.: Scanning rotational Raman lidar at 355 nm for the measurement of tropospheric temperature fields. Atmos. Chem. Phys. 8, 159-169, doi:10.5194/acp-8-159-2008, 2008.

Schutte, B.: Bestimmung von Bodenunterschieden durch Zugkraftmessungen bei der Bodenbearbeitung. Forschungsbericht
655 Agrartechnik des Arbeitskreises Forschung und Lehre der VDI-MEG Nr. 429, 2005.

Santanello Jr, J. A., Dirmeyer, P. A., Ferguson, C. R., Findell, K. L., Tawfik, A. B., Berg, A., Ek, M., Gentine, P., Guillod, B. P., van Heerwaarden, C., Roundy, J., and Wulfmeyer, V.: Land–Atmosphere Interactions: The LoCo Perspective. B. Am. Meteorol. Soc. 99(6), 1253-1272, doi:10.1175/BAMS-D-17-0001.1, 2018.

Schwitalla, T. and Wulfmeyer, V.: Radar data assimilation experiments using the IPM WRF Rapid Update Cycle. Meteorol.
660 Z. 23(1), 79-102, doi:10.1127/0941-2948/2014/0513, 2014.

Seneviratne, S., Lüthi, D., Litschi, M., and Schär, C.: Land–atmosphere coupling and climate change in Europe. Nature 443, 205–209, DOI:10.1038/nature05095, 2006.

Seneviratne, S.I., Corti, T., Davin, E.L., Hirschi, M., Jaeger, E.B., Lehner, I., Orlowsky, B., and Teuling, A.J.: Investigating soil moisture–climate interactions in a changing climate: A review. Earth-Sci. Rev. 99, 125-161,
665 DOI:10.1016/j.earscirev.2010.02.004, 2010.

Singh, D., McDermid, S.P., Cook, B.I., Puma, M.J., Nazarenko, L., and Kelley, M.: Distinct influences of land cover and land management on seasonal climate. J. Geophys. Res.-Atmos. 123, 12017– 12039, DOI:10.1029/2018JD028874, 2018.

Späth, F., A. Behrendt, S. K. Muppa, S. Metzendorf, A. Riede, and V. Wulfmeyer: 3D water vapor field in the atmospheric boundary layer observed with scanning differential absorption lidar. Atmos. Meas. Tech. 9, 1701-1720, doi:10.5194/amt-
670 9-1701-2016, 2016.

Späth, F., Behrendt, A., Brewer, W. A., Lange, D., Senff, C., Turner, D. D., Wagner, T., Wulfmeyer, V.: Simultaneous observations of surface layer profiles of humidity, temperature, and wind using scanning lidar instruments. Journal of Geophysical Research: Atmospheres, 127, e2021JD035697, doi:10.1029/2021JD035697, 2022.

Spuler, S. M., Repasky, K. S., Morley, B., Moen, D., Hayman, M., and Nehrir, A. R.: Field-deployable diode-laser-based differential absorption lidar (DIAL) for profiling water vapor, Atmos. Meas. Tech., 8, 1073–1087, doi:10.5194/amt-8-1073-2015, 2015.

Stevens B., Behrendt, A., Lange, D., Späth, F., Wulfmeyer V., et al.: EURECA4A, Earth Syst. Sci. Data, 13, 4067–4119, doi:10.5194/essd-13-4067-2021, 2021.

Thundathil, R., Schwitalla, T., Behrendt, A., Muppa, S. K., Adam, S., and Wulfmeyer, V.: Assimilation of lidar water vapour mixing ratio and temperature profiles into a convection-permitting model. J. Meteorol. Soc. Jpn. 98(4), doi:10.2151/jmsj.2020-049, 2020.

Thundathil, R., Schwitalla, T., Behrendt, A., and Wulfmeyer, V.: Impact of assimilating lidar water vapour and temperature profiles with a hybrid ensemble transform Kalman filter: Three-dimensional variational analysis on the convection-permitting scale. Q J Roy Meteor Soc, 147(741), 4163–4185, doi:10.1002/qj.4173, 2021.

Turner, D. D., Ferrare, R. A., Brasseur, L. A. H., Feltz, W. F., & Tooman, T. P.: Automated Retrievals of Water Vapor and Aerosol Profiles from an Operational Raman Lidar, Journal of Atmospheric and Oceanic Technology, 19(1), 37-50, doi:10.1175/1520-0426(2002)019<0037:AROWVA>2.0.CO;2, 2002.

Turner, D.D., Wulfmeyer, V., Berg, L.K., and Schween, J.H.: Water vapor turbulence profiles in stationary continental convective mixed layers. J. Geophys. Res. 119, 11151-11165, doi:10.1002/2014JD022202, 2014.

Van den Hurk, B., Doblas-Reye, F., Balsamo, G., Koster, R.D., Seneviratne, S.I., and Camargo Jr, H.: Soil moisture effects on seasonal temperature and precipitation forecast scores in Europe. Clim. Dynam. 38, 349–362, DOI:10.1007/s00382-010-0956-2, 2012.

van Heerwaarden, C.C., Vilà-Guerau de Arellano, J., Moene, A.F., and Holtslag, A.A.M.: Interactions between dry-air entrainment, surface evaporation and convective boundary-layer development. Q. J. Roy. Meteorol. Soc. 135, 1277-1291, DOI:10.1002/qj.431, 2009.

Vilà-Guerau de Arellano, J., Ouwersloot, H.G., Baldocchi, D., and Jacobs, C.M.J.: Shallow cumulus rooted in photosynthesis. Geophys. Res. Lett. 41, 1796–1802, DOI:10.1002/2014GL059279, 2014.

Vogel, M.M., Orth, R., Cheruy, F., Hagemann, S., Lorenz, R., van den Hurk, B.J.J.M., and Seneviratne, S.I.: Regional amplification of projected changes in extreme temperatures strongly controlled by soil moisture-temperature feedbacks. Geophys. Res. Lett. 44, 1511–1519, DOI:10.1002/2016GL071235, 2017.

Vogel, M.M., Zscheischler, J., and Seneviratne, S.I.: Varying soil moisture–atmosphere feedbacks explain divergent temperature extremes and precipitation projections in central Europe. Earth Syst. Dynam. 9, 1107–1125, DOI:10.5194/esd-9-1107-2018, 2018.

Wagner, G., Wulfmeyer, V., Späth, F., Behrendt, A., and Schiller, M.: Performance and specifications of a pulsed high-power single-frequency Ti:Sapphire laser for water-vapor differential absorption lidar. Appl. Optics 52(11), 2454-2469, doi:10.1364/AO.52.002454, 2013.

Warrach-Sagi, K., Schwitalla, T., Wulfmeyer, V., and Bauer, H.-S.: Evaluation of a climate simulation in Europe based on the WRF-N OAH Model System: precipitation in Germany. Clim. Dynam. 41, 755-774, doi:10.1007/s00382-013-1727-7, 2013.

710 Weber, T. K. D., Ingwersen, J., Högy, P., Poyda, A., Wizemann, H.-D., Demyan, M. S., Bohm, K., Eshonkulov, R., Gayler, S., Kremer, P., Laub, M., Nkwain, Y. F., Troost, C., Witte, I., Reichenau, T., Berger, T., Cadisch, G., Müller, T., Fangmeier, A., Wulfmeyer, V., and Streck, T.: Multi-site, multi-crop measurements in the soil–vegetation–atmosphere continuum: a comprehensive dataset from two climatically contrasting regions in southwestern Germany for the period 2009–2018, Earth Syst. Sci. Data, 14, 1153–1181, doi:10.5194/essd-14-1153-2022, 2022.

715 Weckwerth, T. M., Weber, K. J., Turner, D. D., and Spuler, S. M.: Validation of a Water Vapor Micropulse Differential Absorption Lidar (DIAL), Journal of Atmospheric and Oceanic Technology, 33(11), 2353-2372, doi:10.1175/JTECH-D-16-0119.1, 2016.

Wizemann, H.-D., Ingwersen, J., Högy, P., Warrach-Sagi, K., Streck, T., and Wulfmeyer, V.: Three year observations of water vapor and energy fluxes over agricultural crops in two regional climates of Southwest, Germany. Meteorol. Z. 720 24(1), 39-59, doi:10.1127/metz/2014/0618, 2015.

Wulfmeyer, V.: Investigations of humidity skewness and variance profiles in the convective boundary layer and comparison of the latter with large eddy simulation results. J. Atmos. Sci. 56, 1077-1087, doi:10.1175/1520-0469(1999)056<1077:IOHSAV>2.0.CO;2, 1999.

Wulfmeyer, V., Turner, D. D., Pal, S., and Wagner, E.: Can water vapour Raman lidar resolve profiles of turbulent variables 725 in the convective boundary layer? Bound.-Lay. Meteorol. 136, 253-284, doi:10.1007/s10546-010-9494-z, 2010.

Wulfmeyer, V., Hardesty, R. M., Turner, D. D., Behrendt, A., Cadeddu, M. P., Di Girolamo, P., Schlüssel, P., Van Baelen, J., and Zus, F.: A review of the remote sensing of lower-tropospheric thermodynamic profiles and its indispensable role for the understanding and the simulation of water and energy cycles. Rev. Geophys. 53(3), 819–895, doi:10.1002/2014RG000476, 2015.

730 Wulfmeyer, V., Muppa, S. K., Behrendt, A., Hammann, E., Späth, F., Sorbjan, Z., Turner, D. D., and Hardesty, R. M.: Determination of convective boundary layer entrainment fluxes, dissipation rates, and the molecular destruction of variances: Theoretical description and a strategy for its confirmation with a novel lidar system synergy. J. Atmos. Sci. 73(2), 667-692, doi:10.1175/JAS-D-14-0392.1, 2016.

Wulfmeyer, V. , Turner, D.D., Baker, B., Banta, R., Behrendt, A., Bonin, T., Brewer, W. A., Buban, M., Choukulkar, A., 735 Dumas, E., Hardesty, R M., Heus, T., Ingwersen, J., Lange, D., Lee, T. R., Metzendorf, S., Muppa, S. K., Meyers, T., Newsom, R., Osman, M., Raasch, S., Santanello, J., Senff, C., Späth, F., Wagner, T., and Weckwerth, T.: A New research approach for observing and characterizing Land-Atmosphere Feedback. B. Am. Meteorol. Soc., 99(8), 1639-1667, doi:10.1175/BAMS-D-17-0009.1, 2018.

Wulfmeyer, V., Späth, F., Behrendt, A., Jach, L., Warrach-Sagi, K., Ek, M., Turner, D. D., Senff, C., Ferguson, C. R.,
740   Santanello, J., Lee, T. R., Buban, M., and Verhoef, A.: The GEWEX Land-Atmosphere Feedback Observatory
        (GLAFO). GEWEX Quarterly 30, 6-11, https://www.gewex.org/gewex-content/files_mf/1583952472Feb2020.pdf, 2020.

Wulfmeyer V., Senff, C., Späth, F., Behrendt, A., Lange, D., Banta, R. M., Brewer, W. A., Wieser, A., Turner, D. D.:
        Profiling the Molecular Destruction Rates of Temperature and Humidity as well as the Turbulent Kinetic Energy
        Dissipation in the Convective Boundary Layer, in preparation, 2022a.

745   Wulfmeyer, V., Manuel, J., Pineda, V., Otte, S., Karlbauer, M., Butz, M.V., Lee, T.R., Buban, M. and Rajtschan, V.:
        Estimation of the surface fluxes for heat and momentum in unstable conditions with machine learning and similarity
        approaches for the LAFE data set . Bound-Lay. Meteorol., accepted and in press, 2022b.

Zacharias, S., Bogena, H., Samaniego, L., Mauder, M., Fuß, R., Pütz, T. et al.: A network of terrestrial environmental
        observatories in Germany, Vadose Zone Journal, 10(3), 955-973, doi:10.2136/vzj2010.0139, 2011.

750   Zhou, S., Park Williams, A., Berg, A.M., Cook, B.I., Zhang, Y., Hagemann, S., Lorenz, R., Seneviratne, S. I., and Gentine,
        P.: Land–atmosphere feedbacks exacerbate concurrent soil drought and atmospheric aridity. P. Natl. Acad. Sci. 116,
        18848-18853, DOI:10.1073/pnas.1904955116.

Zhou, S., Zhang, Y., Park Williams, A., and Gentine, P.: Projected increases in intensity, frequency, and terrestrial carbon
        costs of compound drought and aridity events. Science Advances 5, eaau5740, DOI:10.1126/sciadv.aau5740, 2019.

755

Table 1 Measured variables with the LAFO sensor synergy. Instruments on bold face are operated continuously. For these instruments we give also the temporal and spatial resolutions; otherwise we refer to the instrument descriptions in Sect. 3 and

760   the corresponding references. RHI scan – range height indicator scanning operation to measure vertical cross-sections.

Instrument, Mode	Soil	Vegetation	Atmosphere	Fluxes	Radiation	Aerosols	Clouds
DIAL, verical			$q(z)$, $dq(z)/dz$, $q'(z)$, $< q'^2>, <q'^3>$			$\beta_{par}(z)$	
DIAL, RHI scan			2D q, dq/dz			2D $\beta_{par}(z)$-field	2D field
RRL, vertical			$T(z)$, $dT(z)/dz$, $T'(z)$, $<T'^2>$, $<T'^3>$, $q(z)$, $dq(z)/dz$, $q'(z)$, $< q'^2>$, $<q'^3>$			$\beta_{par}(z)$, $\alpha_{par}(z)$	Cloud bottom height
RRL, RHI scan			2D T, dT/dz, 2D q, dq/dz			2D $\beta_{par}(z)$, $\alpha_{par}(z)$ field	2D field
DL, vertical 1 s, 30 m			$w(z)$, $w'(z)$, $<w'^2>$, $<w'^3>$, ε			$\beta_{par}(z)$	Cloud bottom height
DL; VAD scan 90 s, 21 m			$V(z)$, dV/dz				
DL, RHI scan			2D wind field			2D $\beta_{par}(z)$-field	2D field
DIAL-DL, vertical							
RRL-DL, vertical							
Two DLs, crosstrack scanning			u, v at the cross points	u^* at the cross point			
DIAL-RRL-DL, RHI			w^*, q^*, T^*	u^*, $L(z)$, $S(z)$			
EC station 30 minutes	$T(-z)$, $q(-z)$, $h(-z)$		T, q, u, v, w, p (all in 2.6 m)	u^*, L_0, S_0, G, Q_n, precipitation	net shortwave		

					and longwave		
UAV, Breedvision	T_S	NDVI, LAI, T_C, z_p, ρ_p, q_p			vis and IR spectra		
WaTSeN 15 minutes	$T(-z)$, $q(-z)$						
in-situ (manual) biweekly		LAI, BBCH, z_p					
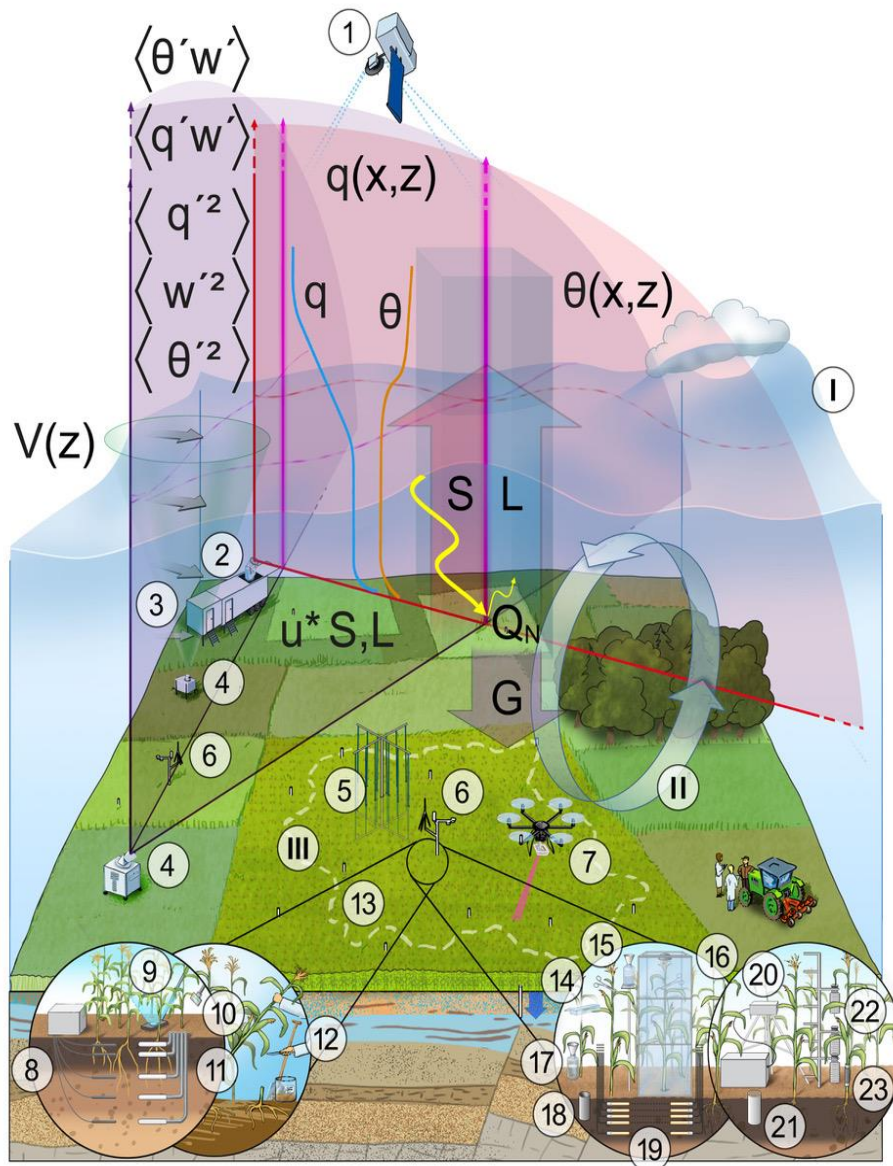
Figure 1 LAFO sensor synergy. I: PBL top, II: mesoscale vortex, III: flux footprint. 1: Satellite remote sensing, 2, 3, 4: vertically staring and scanning Doppler, water vapor, and temperature, lidar systems, 5: 3D fiber optic distributed temperature sensing (FODS) in combination with distributed wind and trace gas sensors, 6: energy balance and eddy covariance stations, 7: unmanned aerial vehicle (UAV), 8: time-domain reflectometers (TDRs), 9: leaf area index (LAI) measurement, 10: gas exchange system for photosynthesis and transpiration rate measurements, 11: tensiometers, 12: in-situ crop measurements such as root and shoot biomass as well as canopy height, 13: soil moisture, temperature, and matric potential network, 14: leaf cuvette, 15: open rainfall sampler, 16: gas exchange chamber, 17: throughfall sampler, 18: groundwater well, 19: in-situ soil water probes (14-19 all coupled to water isotope analyzer), 20: IR gas analyzer, 21: mini lysimeter, 22: canopy temperature, water vapor, and CO_2 profiles, 23: sap flow sensors. For further explanations, see www.gewex.org/panels/global-landatmosphere-system-study-panel/glass-projects and Wulfmeyer et al. (2020).

Figure 2 LAFO experimental site at the Heidfeldhof, locations of the two eddy covariance stations, the 22 soil water content and temperature stations, remote sensing equipment at the lidar site, and extents of agricultural fields. The inlet shows the location of LAFO in Southwest Germany. Basemap source: Esri, DigitalGlobe, GeoEye, Earthstar Geographics, CNES/Airbus DS, USDA, USGS, AeroGRID, IGN, and the GIS User Community.
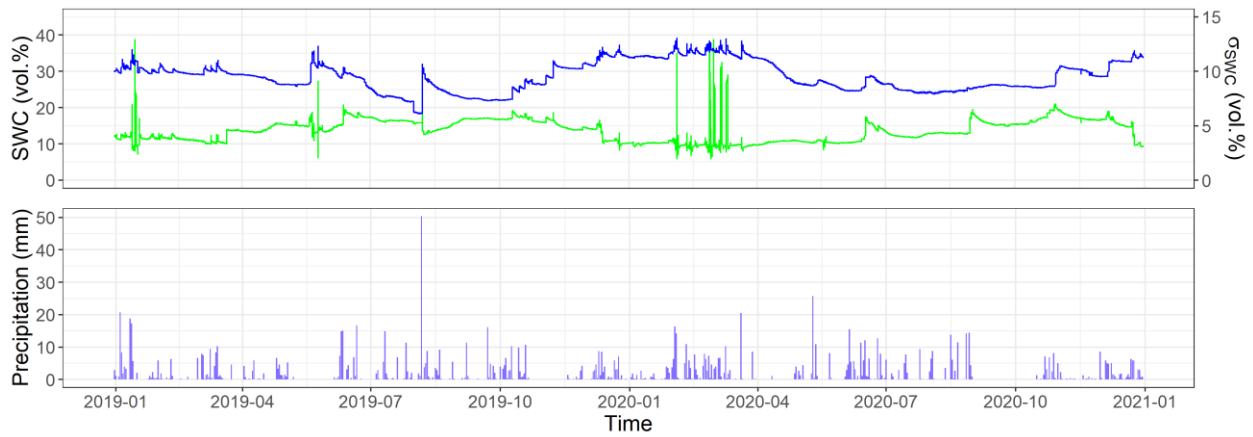
785 **Figure 3** Temporal variations of spatial average soil water content (upper panel, blue), standard deviation of soil water content (upper panel, green), and daily precipitation (bottom panel) with data from WaTSeN during the 2019-2020 years. Soil water content is the spatial mean of daily averaged data from 14 stations of WaTSeN.

790
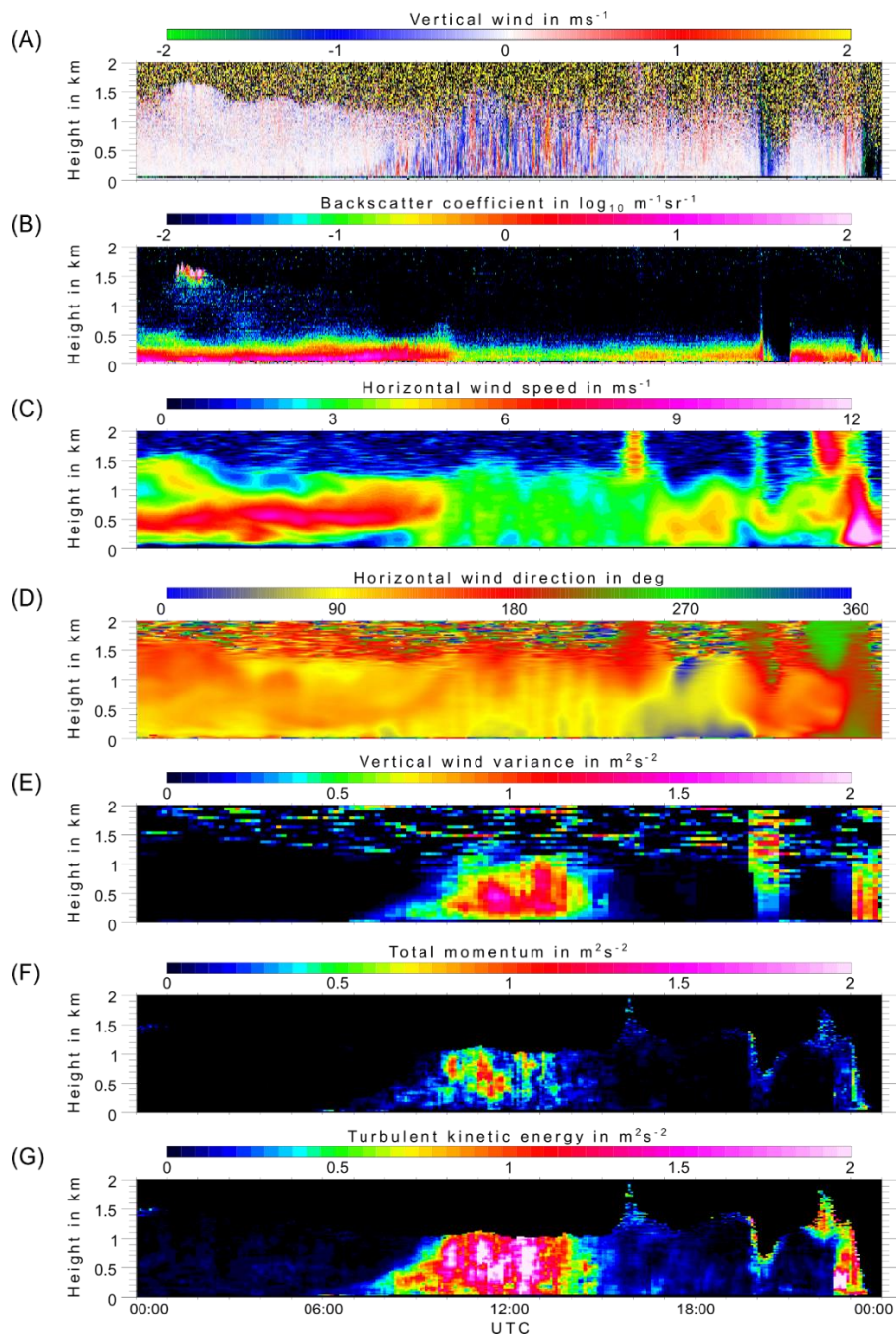
Figure 4 Measurements of the vertical and horizontal wind from 27 June 2021. In addition to the wind itself also the backscatter coefficient, vertical wind variance, TKE and momentum flux are shown.
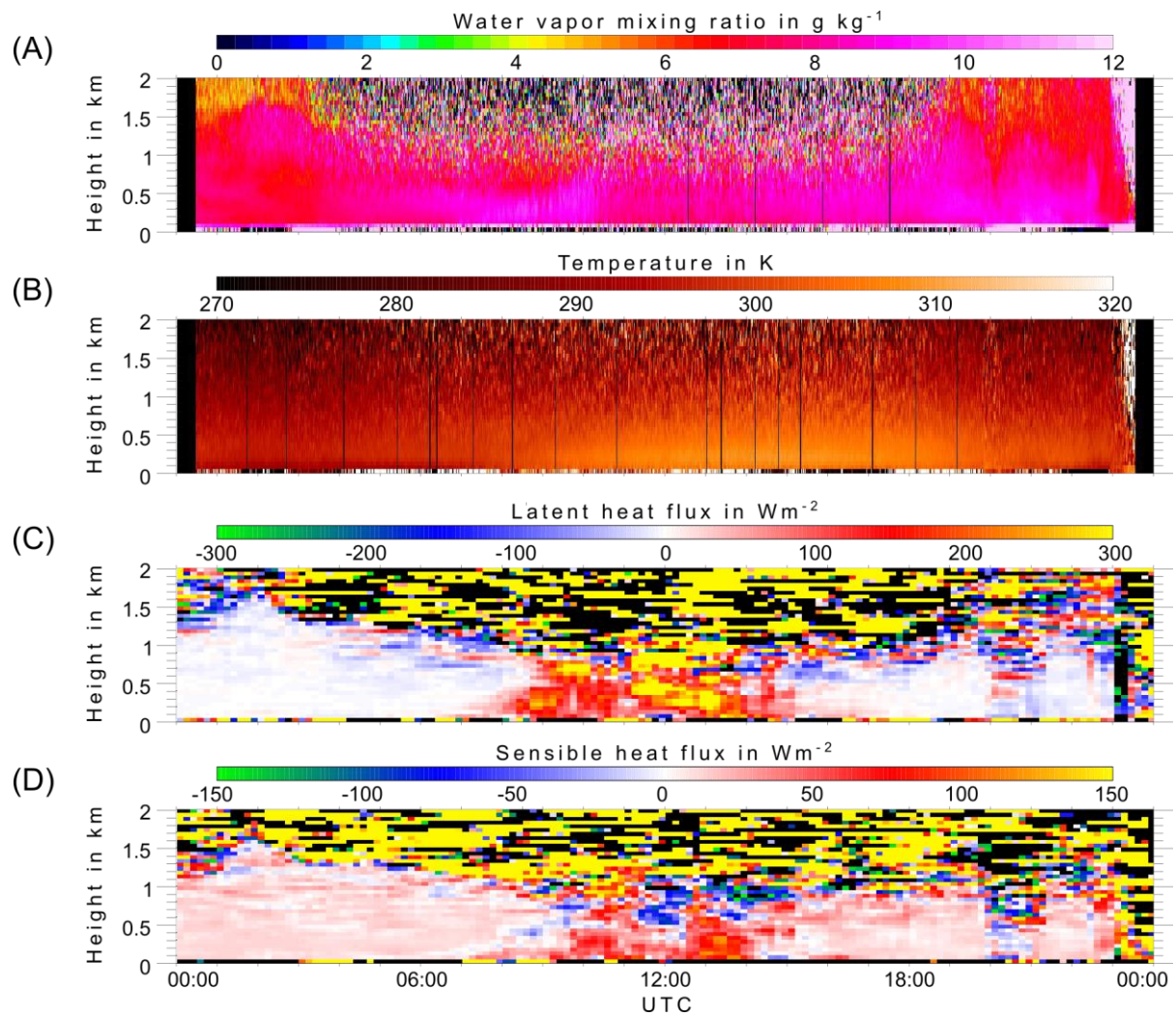
800   **Figure 5** Water vapor mixing ratio and temperature time-series for 27 June 2021 are plotted in (A) and (B). In (C) and (D) the latent and sensible heat fluxes are shown for that day.
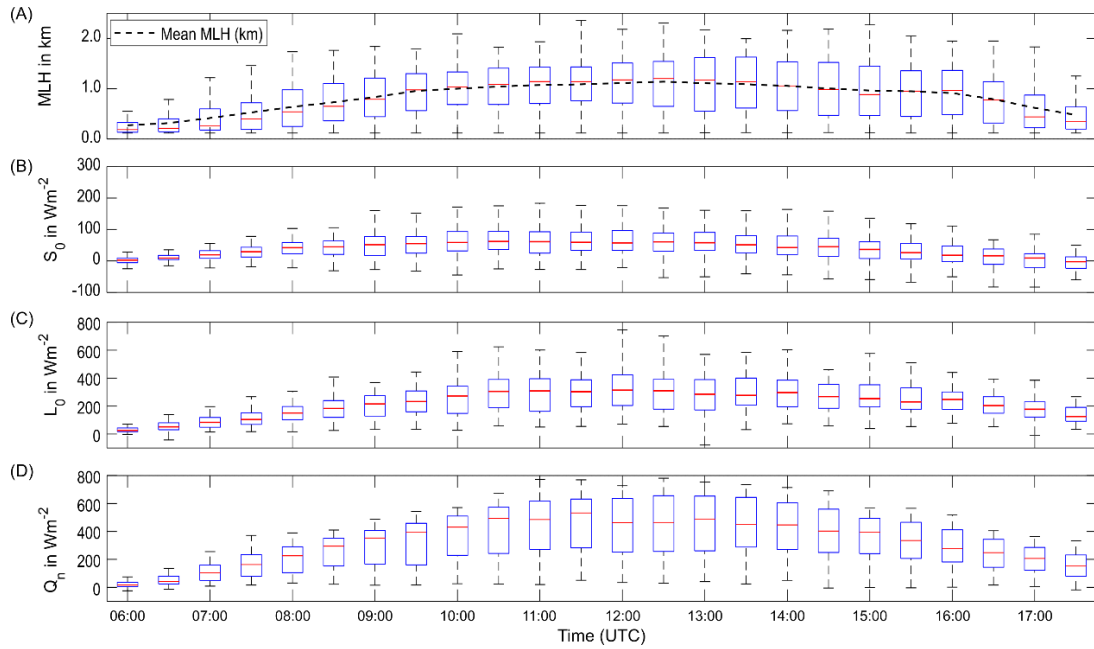
805

Figure 6 Statistics of the diurnal cycle between 6 and 18 UTC of mixing layer height MLH (A), surface sensible heat flux S_0 (B) and latent heat fluxe L_0 (C), and net radiation Q_n. (D) for three months from May to July 2021.
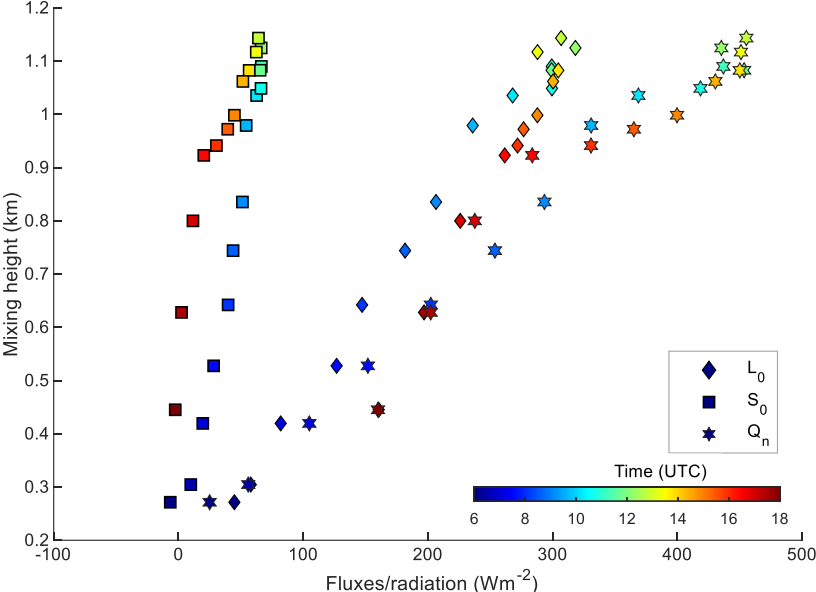
Figure 7 Correlation of the mixing layer height MLH with the surface sensible and latent heat fluxes S_0 and L_0 and the net radiation Q_n. The color indicates the time of the day.
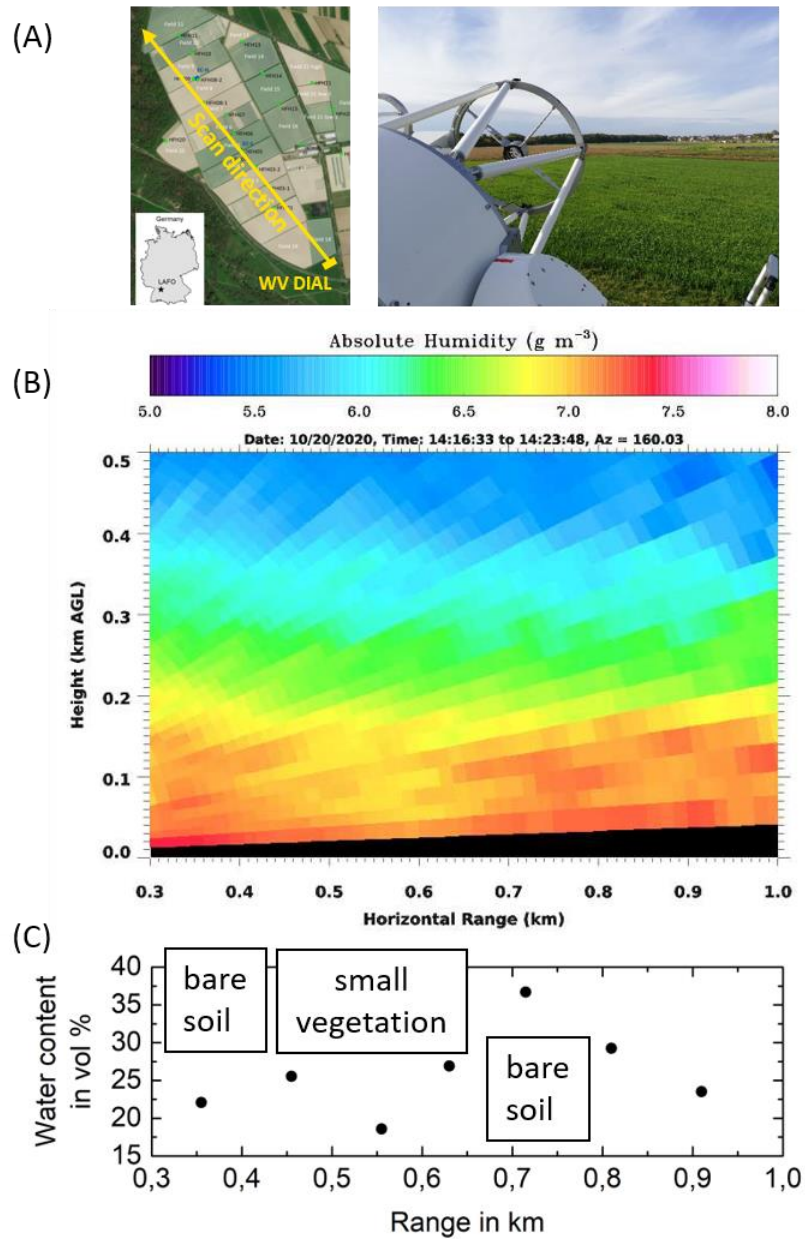
Figure 8 Scanning WV DIAL measurements over the agricultural field of Heidfeldhof on 20 October 2020 between 14:23 and 14:31 UTC. (A) shows the scan direction to the north-west with a picture from the scanner over the agricultural fields. (B) gives the humidity field in the lowest 0.5 km above ground (with respect to the altitude of the lidar site). (C) shows the soil water content values in 40 cm depth from WaTSeN along the scan direction. Basemap source in (A): Esri, DigitalGlobe, GeoEye, Earthstar Geographics, CNES/Airbus DS, USDA, USGS, AeroGRID, IGN, and the GIS User Community.